Numerical Methods for Acoustic Problems with Complex Geometries Based on Cartesian Grids

D.N. Vedder
1103784
Rusthoflaan 94b
3034 XP Rotterdam

Supervisors:

Dr. ir. C. Vuik
Prof. dr. ir. P. Wesseling
Delft University of Technology, The Netherlands

Clarence L. "Kelly" Johnson Collegiate Professor
W. Shyy
University of Michigan, USA

November 21, 2005

Abstract

Computational AeroAcoustics deals with both disciplines Computational Fluid Dynamics and AeroAcoustics. Acoustic propagation problems are governed by the linearized Euler equations. All properties of the acoustic waves are encoded in the dispersion relation of these equations. Optimized high order numerical schemes are presented in this report. These schemes optimize the dispersion and dissipation errors by preserving the dispersion relation and are presented in the original finite difference and the finite volume approach.

In many practical applications complex geometries have to be handled. This report presents a cut-cell method, which uses a Cartesian background grid. In the interior of the domain the numerical schemes can easily be implemented but in the vicinity of the boundaries special treatment for each cell is required.

To test this approach, a testcase with results is presented. Furthermore, proposals for further investigation are presented. Investigation of the resulting order of accuracy and the impact of the cut-cell method on it are proposed. Also an improvement of the numerical solution by Richardson extrapolation or least square extrapolation is proposed.

Contents

1 Acoustic Models **3**
- 1.1 Introduction . . . 3
- 1.2 The Wave Equation and Acoustic Analogies . . . 5
  - 1.2.1 Linear Acoustic Wave Equation . . . 5
  - 1.2.2 Lighthill Acoustic Analogy . . . 6
  - 1.2.3 Ffowcs Williams - Hawkings Analogy . . . 7
- 1.3 Problem . . . 9

2 Numerical Methods **11**
- 2.1 Introduction . . . 11
- 2.2 Dispersion-Relation-Preserving Scheme . . . 12
  - 2.2.1 Finite Difference approach . . . 12
  - 2.2.2 Finite Volume approach . . . 15
  - 2.2.3 Time Integration . . . 16
  - 2.2.4 Stability . . . 18
- 2.3 Optimized Prefactored Compact Scheme . . . 19
  - 2.3.1 Finite Difference approach . . . 19
  - 2.3.2 Finite Volume approach . . . 23
  - 2.3.3 Time Integration . . . 24
  - 2.3.4 Stability . . . 27
- 2.4 Cut-Cell Method . . . 28
  - 2.4.1 Ordinary Second Order Cut-Cell Method . . . 28
  - 2.4.2 Cut-Cell Method for CAA Approach . . . 31

3 Conclusions and Future Work **33**
- 3.1 Introduction . . . 33
- 3.2 Results . . . 33
- 3.3 Future work . . . 35
  - 3.3.1 Proposals . . . 35
  - 3.3.2 Richardson Extrapolation . . . 36

4 References **37**

5 Appendix **38**

1 Acoustic Models

1.1 Introduction

Computational AeroAcoustics (CAA) deals with both disciplines Computational Fluid Dynamics and AeroAcoustics. Sound generated by aerodynamic forces or a flow, fall in the category of aeroacoustics. Aeroacoustics should not be confused with classical acoustics, e.g. sound generated by loudspeakers is in the domain of classical acoustics, whereas sound generated by a turbulent flow is in the aeroacoustic area.

An acoustic wave has a wavelength λ in space, as well as a frequency f in time. The speed of sound in a medium is c_0. These are coupled by the following relation: $\lambda f = c_0$. It is well known that all wave propagation properties are encoded in the dispersion relation of the governing equations [8,9]. The dispersion relation is a relation between the angular frequency $\omega = 2\pi f$ and the wavenumber of the wave $\alpha = \frac{2\pi}{\lambda}$. This relation can easily be obtained by taking space and time Fourier transforms of the governing equations. For example, the dispersion relation of the one-dimensional wave equation is:

$$\frac{\partial^2 u}{\partial t^2} - c_0^2 \frac{\partial^2 u}{\partial x^2} = 0 \qquad \Rightarrow \qquad \omega^2 = c_0^2 \alpha^2 \qquad \Rightarrow \qquad \omega = \pm c_0 \alpha = W(\alpha),$$

with angular frequency ω and wavenumber α.

Also dispersiveness (spreading), dissipativeness (damping), group velocity ($v_{gr} = \frac{dW}{d\alpha}$), phase velocity ($v_{ph} = \frac{W(\alpha)}{\alpha}$) etc. are all determined by the dispersion relation, e.g. when v_{ph} depends on α the waves are dispersive and when $W(\alpha)$ has an imaginary part the waves are dissipative [8,9].

It is well-known that acoustic waves are non-dispersive. Although sound is dissipated by viscosity, it is dissipated after a very long travel distance and therefore acoustics is considered to be an inviscid fluid phenomenon. So, dissipative loss becomes important for sound with high frequencies, which travels long distances. It is also well-known that acoustic waves travel with the speed of sound. In order to commit satisfactory CAA all wave properties have to be preserved in the numerical solution, which implies low dispersion and dissipation error. This can be obtained by preserving the dispersion relation in the numerical scheme, which can be done by preserving the wavenumber and the angular frequency. So when a numerical scheme has the same dispersion relation as the governing equations, the waves in the numerical solution will have the same properties as those of the governing equation.

Many CFD schemes are dispersive and dissipative. Sometimes numerical dissipation is added to make the scheme stable. In CFD, schemes are usually assessed by the order of Taylor series truncation, higher order often means better local approximation, and by the Lax theorem for convergence. In acoustics all this does not ensure a good quality numerical solution, as appears from the previous discussion. A common approach in CFD is to make a stretched grid, e.g. boundary layers. In acoustics stretched grids could cause strange phenomena, such as change of frequency or even reflection [2].

Another difficulty in CAA are the type of problems for practical applications. These problems often are exterior problems, what implies that these problems have to be solved in an unbounded space. Thus for computational sake, the space has to be cut off to make the computational domain finite. Boundary conditions have to be proposed for those cut off boundaries. The boundary conditions are outflow boundary conditions for the free space behind, which implies that reflection of outgoing waves is undesirable.

Also problems in acoustics often have complex geometries. So, good methods to handle these complexities are required.

Like explained before, sound propagation is modelled as an inviscid fluid phenomenon. On the other hand, if sound generation by a flow is considered, viscosity (implying the Reynolds number) plays an important role. Sound is mainly generated in turbulent flows, e.g. acceleration of vorticity.

In the remaining of Chapter 1 important sound propagation and generation models are derived. Also an acoustic problem is posed in this chapter. In Chapter 2 numerical methods are discussed. Here the DRP and OPC spatial discretization scheme is presented respectively in Section 2.1 and 2.2. Also time integration schemes are included. To handle complex geometries the cut-cell method is presented in Section 2.3. Conclusions and future work are discussed in Chapter 3.

1.2 The Wave Equation and Acoustic Analogies

Aeroacoustics is concerned with sound propagation and generation. This is mainly done for fluids such as air and water, which have small viscosity and heat conduction. Also disturbances are very small. For the propagation of sound dissipative effects have to be taken into account after very long travel distances. So sound is generally considered as an inviscid fluid phenomenon. Therefor Euler's equation will be used to derive the wave equation in the first subsection. In the second subsection Lighthill's acoustic analogy is derived by rearranging the equations of fluid dynamics. This analogy deals with sound generated by a turbulent flow and its propagation and has its main application in flows without solid boundaries or more correctly, the effects of solid boundaries can be neglected. As an extension of Lighthill's analogy the Ffowcs Williams Hawkings equation is derived in the third subsection. This equation deals with sound generation and propagation in a turbulent flow in presence of solid boundaries.

1.2.1 Linear Acoustic Wave Equation

This equation is derived for a homogeneous fluid with characteristics:

$$\rho = \rho_0, \qquad p = p_0, \qquad \boldsymbol{u} = 0,$$

where $\boldsymbol{u}$ represents a vector and ρ_0 and p_0 are constants.
When sound disturbs the fluid, the fluid is characterized by:

$$\begin{array}{ll} \rho = \rho_0 + \rho', & |\rho| \ll \rho_0, \\ p = p_0 + p', & |p'| \ll \rho_0 c_0^2, \\ \boldsymbol{u} = \boldsymbol{u}', & \|\boldsymbol{u}'\| \ll c_0. \end{array} \tag{1}$$

The Euler equation (momentum equation for an inviscid flow) and the equation of state are used to obtain the wave equation:

$$\begin{array}{l} \rho_t + \boldsymbol{u} \cdot \nabla\rho + \rho\nabla \cdot \boldsymbol{u} = 0, \\ \rho(\boldsymbol{u}_t + (\boldsymbol{u} \cdot \nabla)\boldsymbol{u}) + \nabla p = 0, \end{array} \tag{2}$$

and

$$p' = c_0^2 \rho', \tag{3}$$

where c_0 is the propagation speed (speed of sound).
Substituting (1) into (2) leads to:

$$\begin{array}{l} (\rho_0 + \rho')_t + \boldsymbol{u}' \cdot \nabla(\rho_0 + \rho') + (\rho_0 + \rho')\nabla \cdot \boldsymbol{u}' = \\ {\rho'}_t + \boldsymbol{u}' \cdot \nabla\rho' + \rho_0 \nabla \cdot \boldsymbol{u}' + \rho' \nabla \cdot \boldsymbol{u}' = 0, \end{array} \tag{4}$$

and

$$\begin{array}{l} (\rho_0 + \rho')\left[{\boldsymbol{u}'}_t + (\boldsymbol{u}' \cdot \nabla)\boldsymbol{u}'\right] + \nabla(p_0 + p') = \\ \rho_0 {\boldsymbol{u}'}_t + \rho' {\boldsymbol{u}'}_t + \rho_0(\boldsymbol{u}' \cdot \nabla)\boldsymbol{u}' + \rho'(\boldsymbol{u}' \cdot \nabla)\boldsymbol{u}' + \nabla p' = 0. \end{array} \tag{5}$$

All perturbation are small, so higher order terms can be neglected, which results in the following:

$$\rho'_t + \rho_0 \nabla \cdot \boldsymbol{u}' = 0, \tag{6}$$

$$\rho_0 \boldsymbol{u}'_t + \nabla p' = 0. \tag{7}$$

From (3) it follows that $\nabla p' = c_0^2 \nabla \rho'$, which can be substituted in (7):

$$\rho'_t + \rho_0 \nabla \cdot \boldsymbol{u}' = 0, \tag{8}$$

$$\rho_0 \boldsymbol{u}'_t + c_0^2 \nabla \rho' = 0. \tag{9}$$

Note that (8) and (9) are the linearized Euler equations.

Now the time derivative of (8) and the divergence of (9) have to be taken:

$$\rho'_{tt} + \rho_0 \nabla \cdot \boldsymbol{u}'_t = 0, \tag{10}$$

$$\rho_0 \nabla \cdot \boldsymbol{u}'_t + c_0^2 \nabla^2 \rho' = 0. \tag{11}$$

which is equivalent with:

$$\rho'_{tt} + \rho_0 \nabla \cdot \boldsymbol{u}'_t = 0, \tag{12}$$

$$\rho_0 \nabla \cdot \boldsymbol{u}'_t = -c_0^2 \nabla^2 \rho'. \tag{13}$$

Substituting (13) into (12) gives the wave equation:

$$\rho'_{tt} - c_0^2 \nabla^2 \rho' = 0. \tag{14}$$

This can be uniquely solved with two initial and two boundary conditions.

1.2.2 Lighthill Acoustic Analogy

In this section the acoustic approach introduced by Lighthill is derived. This approach is used to calculate acoustic radiation from a turbulent flow in an infinite homogeneous fluid with reference values ρ_0, c_0 and p_0.

Density and pressure fluctuations are defined as in the previous subsection.

The summation convention is used to write the continuity and momentum equations:

$$\frac{\partial \rho}{\partial t} + \frac{\partial}{\partial x_j}(\rho u_j) = 0. \tag{15}$$

$$\rho \left(\frac{\partial u_i}{\partial t} + u_j \frac{\partial u_i}{\partial x_j} \right) = -\frac{\partial p}{\partial x_i} + \frac{\partial \sigma_{ij}}{\partial x_j}, \tag{16}$$

where σ_{ij} is the component of the viscous stress tensor.

Multiplying (15) by u_i and adding this to (16) gives:

$$\begin{array}{ccccc} \underbrace{\rho \dfrac{\partial u_i}{\partial t} + u_i \dfrac{\partial \rho}{\partial t}} & & + \underbrace{\rho u_j \dfrac{\partial u_i}{\partial x_j} + u_i \dfrac{\partial}{\partial x_j}(\rho u_j)} & = & -\frac{\partial p}{\partial x_i} + \frac{\partial \sigma_{ij}}{\partial x_j}, \\ \frac{\partial}{\partial t}(\rho u_i) & + & \frac{\partial}{\partial x_j}(\rho u_i u_j) & = & -\frac{\partial p}{\partial x_i} + \frac{\partial \sigma_{ij}}{\partial x_j}. \end{array} \tag{17}$$

This can be written in the following way:

$$\frac{\partial}{\partial t}(\rho u_i) = -\frac{\partial}{\partial x_j}(\rho u_i u_j) - \frac{\partial p}{\partial x_i} + \frac{\partial \sigma_{ij}}{\partial x_j} = -\frac{\partial}{\partial x_j}(\rho u_i u_j + \delta_{ij} p - \sigma_{ij}). \tag{18}$$

Adding $c_0^2 \frac{\partial \rho}{\partial x_i}$ to both sides:

$$\frac{\partial}{\partial t}(\rho u_i) + c_0^2 \frac{\partial \rho}{\partial x_i} = -\frac{\partial}{\partial x_j}(\rho u_i u_j + \delta_{ij}(p - c_0^2 \rho) - \sigma_{ij}). \tag{19}$$

The divergence of this equation is as follows:

$$\frac{\partial}{\partial x_i}\frac{\partial}{\partial t}(\rho u_i) + c_0^2 \frac{\partial^2 \rho}{\partial x_i^2} = -\frac{\partial^2}{\partial x_i \partial x_j}(\rho u_i u_j + \delta_{ij}(p - c_0^2 \rho) - \sigma_{ij}). \tag{20}$$

Time differentiation of the continuity equation (15) gives:

$$\frac{\partial^2 \rho}{\partial t^2} + \frac{\partial}{\partial t}\frac{\partial}{\partial x_j}(\rho u_j) = 0. \tag{21}$$

Substracting (20) of (21):

$$\frac{\partial^2 \rho}{\partial t^2} + \left[\frac{\partial}{\partial t}\frac{\partial}{\partial x_j}(\rho u_j) - \frac{\partial}{\partial x_i}\frac{\partial}{\partial t}(\rho u_i)\right] - c_0^2 \frac{\partial^2 \rho}{\partial x_i^2} = \frac{\partial^2 (\rho u_i u_j + \delta_{ij}(p - c_0^2 \rho) - \sigma_{ij})}{\partial x_i \partial x_j}. \tag{22}$$

Because p_0, ρ_0 and c_0 are constant, the final equation can be written as follows:

$$\frac{\partial^2 \rho'}{\partial t^2} - c_0^2 \nabla^2 \rho' = \frac{\partial^2 T_{ij}}{\partial x_i \partial x_j}\,, \tag{23}$$

where $T_{ij} = \rho u_i u_j + \delta_{ij}\left[(p - p_0) - c_0^2(\rho - \rho_0)\right] - \sigma_{ij}$ is Lighthill's turbulence stress tensor.

Equation (23) clearly has the same form as the classical wave equation. In analogy with classical acoustics this is a wave equation that governs the acoustic field produced by a quadrupole source of strength T_{ij} [10].

1.2.3 Ffowcs Williams - Hawkings Analogy

In this section the acoustic approach introduced by Ffowcs Williams and Hawkings is derived. This approach deals with the presence of rigid bodies in the flow. The most important assumption is that there is no flow-acoustics coupling, this means that the acoustics don't affect the flow.

Consider a finite volume with a moving rigid body, which is described as a mathematical surface $S(t)$ with $f(x,t)$ defined as the kinematics of this surface. On every point on the surface the velocity $\boldsymbol{u_s}$ and the unit normal vector $\boldsymbol{n}$ are defined. Inside this rigid body the flow is perfectly at rest. An example of a geometry is shown in Figure 1.

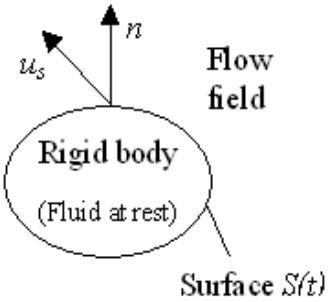

Figure 1: Geomety of a flow field
with a moving rigid body.

The no cross-flow condition on the surface can be decribed as follows:

$$\boldsymbol{u}_s \cdot \boldsymbol{n} = \boldsymbol{u} \cdot \boldsymbol{n}, \tag{24}$$

where $\boldsymbol{u}$ is the velocity of the surrounding fluid.

With the presence of the rigid bodies the continuity and momentum equations are modified. This is because in vicinity of the surface the mass and momentum balances are different. The continuity and momentum equations can be written as follows:

$$\frac{\partial \rho}{\partial t} + \frac{\partial}{\partial x_j}(\rho u_j) = \rho_0 u_{s,i} \delta(f) \frac{\partial f}{\partial x_i}, \tag{25}$$

$$\frac{\partial}{\partial t}(\rho u_i) + \frac{\partial}{\partial x_j}(\rho u_i u_j - \sigma_{ij}^{'}) = -\sigma_{ij}^{'} \delta(f) \frac{\partial f}{\partial x_j}, \tag{26}$$

where δ is the Dirac delta function and $\sigma_{ij}^{'} = \sigma_{ij} - (p - p_0)\delta_{ij}$ with σ_{ij} the viscous stress tensor and p the static pressure.

Following the same procedure as in Lighthill's analogy the following is obtained:

$$\frac{\partial^2 \rho'}{\partial t^2} - c_0^2 \nabla^2 \rho' = \frac{\partial^2 T_{ij}}{\partial x_i \partial x_j} + \frac{\partial}{\partial x_i}\left(\sigma_{ij}^{'} \delta(f) \frac{\partial f}{\partial x_j}\right) + \frac{\partial}{\partial t}\left(\rho_0 u_{s,i} \delta(f) \frac{\partial f}{\partial x_i}\right). \tag{27}$$

Roger [ref] showed that fluctuations in the fluid are exactly the same as the fluctuations that would appear in an equivalent medium at rest. These fluctuations are forced by the following source distributions:

1. A volume distribution $\frac{\partial^2 T_{ij}}{\partial x_i \partial x_j}$ in the real flow field due to the flow.

2. A surface distribution $\frac{\partial}{\partial x_i}\left(\sigma_{ij}^{'} \delta(f) \frac{\partial f}{\partial x_j}\right)$ due to the interaction of the flow with the moving boundaries.

3. A surface distribution $\frac{\partial}{\partial t}\left(\rho_0 u_{s,i} \delta(f) \frac{\partial f}{\partial x_i}\right)$ due to the kinematics of the bodies.

1.3 Problem

From the derivation of the homogeneous wave equation it appears that the linearized Euler equations are used to model acoustic propagation. The following acoustic problem has been posed by Popescu, Shyy and Tai [11]. The problem is solved in 2-D and has a geometry as in Figure 2.

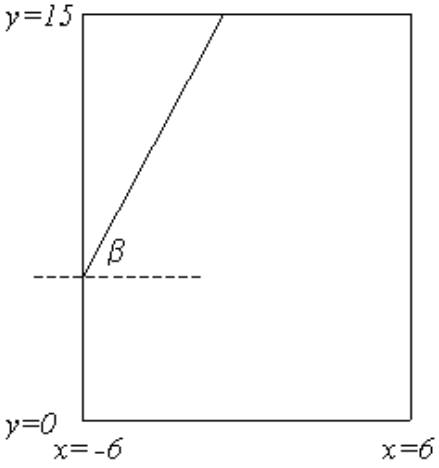

Figure 2: Geometry of the problem.

For this problem the computational domain is $(x, y) \in [-6, 6] \times [0, 15]$, which is cut off by a solid wall, defined by α. At $y = 0$ and around $x = 0$ a piston, that is baffled, is located. The problem is to find the sound field generated by this baffled piston. This field is reflected by the solid wall. The problem is modelled as follows:

1. The linearized Euler equations are used, which are non-dimensionalized with $c_0 = 1$:

$$\begin{array}{c} \frac{\partial p}{\partial t} + \nabla \cdot \boldsymbol{u} = 0, \\ \frac{\partial \boldsymbol{u}}{\partial t} + \nabla p = 0, \end{array} \tag{28}$$

   where $\boldsymbol{u} = \binom{u}{v}$.

2. The initial conditions are as follows:

$$\begin{array}{c} \boldsymbol{u} = 0, \\ p = 0. \end{array} \tag{29}$$

3. The boundary conditions are as follows:

$$v(x, 0, t) = \begin{cases} V_0 \cos(\omega t), & (x, 0) \in piston \\ 0, & otherwise \end{cases} \tag{30a}$$

   where $V_0 = 1$ and $\omega = 4$.

$$\left.\begin{array}{l} \boldsymbol{u}_n = 0 \\ \frac{\partial p}{\partial n} = 0 \end{array}\right\} \quad \text{on the solid wall.} \tag{30b}$$

$$\text{Outflow conditions at } x = -6,\ x = 6 \text{ and } y = 15. \tag{30c}$$

The goal is to solve this problem numerically. Several methods are presented in the following chapters to obtain satisfactory numerical solutions. Results of Popescu, Shyy and Tai [11] are presented in Chapter 3.

2 Numerical Methods

2.1 Introduction

In the previous chapter it has been shown that acoustic propagation problems can be modelled by the linearized Euler equations. Properties of the acoustic waves, such as dispersiveness, dissipativeness, speed of sound etc. have to be preserved in the numerical solution. In order to obtain such a satisfactory numerical solution, low dispersion and low dissipation errors are required. The dispersion relation of the governing equations contains all characteristics of the waves. Waves of the numerical solution should have the same properties as those of the linearized Euler equations. To obtain this, the dispersion relation of the numerical solution should be equal to the one of the linearized Euler equations. Several numerical schemes have been introduced to preserve this dispersion relation in combination with a satisfactory order of accuracy. In this chapter the Dispersion-Relation-Preserving and Optimized-Prefactored-Compact scheme are presented, both in the original finite difference approach followed by the finite volume approach. A finite volume approach has been developed to handle better non-linearities and complex geometries, which are often present in practical applications. Also optimized time integration schemes and a stability analysis are presented.

In this chapter also a cut-cell method is presented. This method uses a Cartesian background grid, therefore the presented schemes can easily be implemented in the interior. In the vicinity of the complex boundaries the cut-cell approach handles the irregular boundary cells. To preserve the order of accuracy of the schemes, used in the interior, the cut-cell method should have the same order of accuracy. First an ordinary cut-cell method is presented followed by a higher order cut-cell method for acoustic problems.

2.2 Dispersion-Relation-Preserving Scheme

Acoustic problems are governed by the linearized Euler equations. In the dispersion relation of these equations all characteristics are encoded. To obtain a satisfactory numerical solution the result must contain waves with the same characteristics as those of the linearized Euler equations. This ensures low dispersion and low dissipation errors. So, the DRP scheme's main goal is to match the discrete and continuous dispersion relations.

2.2.1 Finite Difference approach

Tam [1] introduced a DRP-scheme in a finite differences approach. This scheme is constructed as follows:

$$\frac{du}{dx}(x) \simeq \frac{1}{\Delta x} \sum_{j=-N}^{N} a_j u(x + j\Delta x). \tag{31}$$

This approximation uses $2N + 1$ nodes. There are two important goals to make a good scheme:

1. It has an order of accuracy of $2(N - 1)$. So, $\frac{du}{dx}(x) - \frac{1}{\Delta x} \sum_{j=-N}^{N} a_j u(x + j\Delta x) = O(\Delta x^{2(N-1)})$.
2. The behaviour of the numerical solution must be close to that of the exact solution.

Fourier transforms are used in this derivation. Fourier transform with wavenumber $\alpha \in \mathbb{R}$, is defined as:

$$\widetilde{f}(\alpha) = \frac{1}{2\pi} \int_{-\infty}^{\infty} f(x) e^{-i\alpha x} dx, \tag{32}$$

and its inverse:

$$f(x) = \int_{-\infty}^{\infty} \widetilde{f}(\alpha) e^{i\alpha x} d\alpha. \tag{33}$$

The Fourier transform leads to the following derivative and shift theorems:

$$\begin{aligned} \widetilde{\frac{\partial f}{\partial x}(x)} &= i\alpha \widetilde{f}(\alpha), \\ \widetilde{f(x + \lambda)} &= e^{i\alpha\lambda} \widetilde{f}(\alpha). \end{aligned} \tag{34}$$

Applying this to (31) the following expression is obtained:

$$i\alpha\widetilde{u} = \frac{1}{\Delta x} \left[\sum_{j=-N}^{N} a_j e^{ij\alpha\Delta x} \right] \widetilde{u} = i\overline{\alpha}\widetilde{u}, \tag{35}$$

where the wavenumber of the scheme $\overline{\alpha}$ is defined as follows:

$$\overline{\alpha} = \frac{-i}{\Delta x}\left[\sum_{j=-N}^{N} a_j e^{ij\alpha\Delta x}\right]. \tag{36}$$

Note that $\overline{\alpha}$ is a periodic function of $\alpha\Delta x$. To match $\overline{\alpha}$ and α a first condition is: $\overline{\alpha} \in \mathbb{R}$. This implies that the coefficients a_j must be anti-symmetric ($a_j = -a_{-j}$) and $a_0 = 0$. Plugging these identities into the scheme's wavenumber gives:

$$\overline{\alpha} = \frac{1}{\Delta x}\left[\sum_{j=1}^{N} 2a_j \sin(j\alpha\Delta x)\right]. \tag{37}$$

This looks like a truncated Fourier sine series. So, this scheme tries to approximate the derivative by a truncated Fourier sine series in the wavenumber space.

To have an order of accuracy of $2(N-1)$ a Taylor expansion of (31) can be made:

$$\Delta x\frac{du}{dx} \simeq \sum_{j=-N}^{N} a_j\left(u(x) + j\Delta x\frac{du}{dx} + ... + \frac{(j\Delta x)^{2N-3}}{(2N-3)!}\frac{d^{2N-3}u}{dx^{2N-3}} + \frac{(j\Delta x)^{2(N-1)}}{2(N-1)!}\frac{d^{2(N-1)}u}{dx^{2(N-1)}} + ...\right). \tag{38}$$

With the anti-symmetric property of a_j only the odd terms of this Taylor expansion give $N-1$ conditions for N unknowns. This leaves only one parameter as a free parameter, say a_k.

Now, a second condition can be derived to match α and $\overline{\alpha}$. This is done by choosing the free a_k such that the error is minimized over a specified wavenumber range. The error E is defined as:

$$E = \int_{-\eta}^{\eta} (\alpha\Delta x - \overline{\alpha}\Delta x)^2 d(\alpha\Delta x) = \int_{-\eta}^{\eta}\left[y - \sum_{j=1}^{N} 2a_j \sin(jy)\right]^2 dy. \tag{39}$$

Note that: $\min_{a_k} E \quad \Leftrightarrow \quad \frac{\partial E}{\partial a_k} = 0.$

Tam [1] showed that for $\eta = \frac{\pi}{2}$ the coefficients of the 4^{th} order scheme are:

$a_0 = 0,$
$a_1 = -a_{-1} = 0.79926643,$
$a_2 = -a_{-2} = -0.18941314,$
$a_3 = -a_{-3} = 0.02651995.$

Figure 3 [2] shows $\overline{\alpha}\Delta x$ as a function of $\alpha\Delta x$. Also the ideal situation $\overline{\alpha}\Delta x = \alpha\Delta x$ for all $\alpha\Delta x$ is shown.

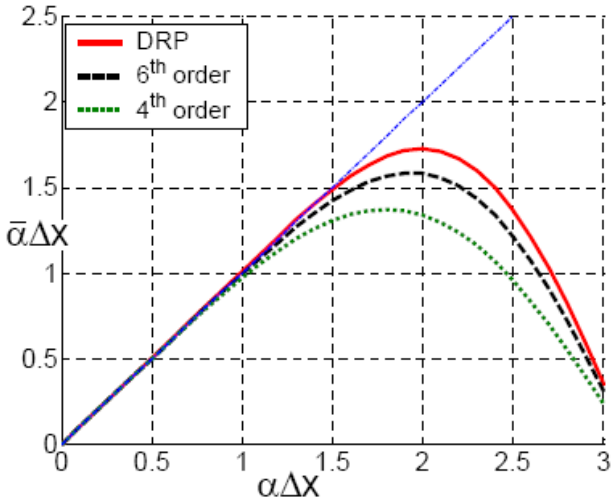

Figure 3: $\alpha\Delta x$ versus $\overline{\alpha}\Delta x$ for the DRP 4^{th} order scheme and two standard 4^{th} and 6^{th} order schemes.

The value of α_c can be determined by the condition $|\alpha\Delta x - \overline{\alpha}\Delta x| < 0.001$, for example. This means that this scheme produces quite accurate results for wavenumbers less than α_c. From Figure 2 it appears that $\alpha\Delta x$ and $\overline{\alpha}\Delta x$ are nearly the same up to $\alpha\Delta x$ is $\alpha_c\Delta x$ for the DRP scheme.

Another important issue to consider the performance of the scheme is the group velocity $\frac{d\overline{\alpha}}{d\alpha}$. This should be nearly one to avoid dispersion in wave propagation. In Figure 4 [2] it appears that by narrowing the range of wavenumbers dispersion can be reduced.

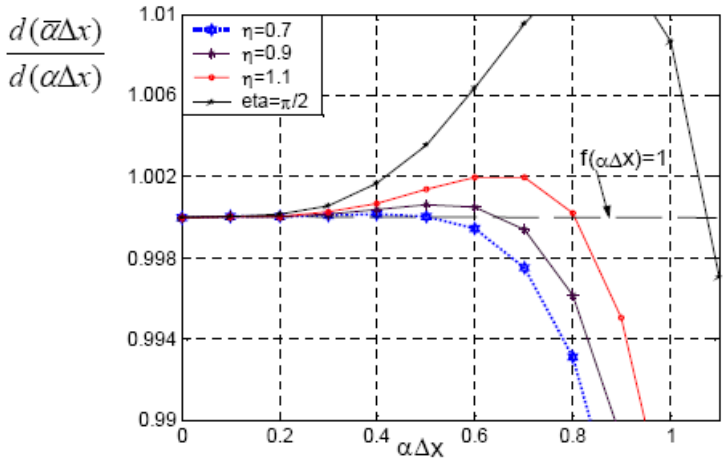

Figure 4: $\frac{d(\overline{\alpha}\Delta x)}{d(\alpha\Delta x)}$ versus $\alpha\Delta x$ for the 4^{th} order DRP scheme.

2.2.2 Finite Volume approach

In many practical applications problems are posed with complex geometries and non-linearities. In order to better handle these non-linearities and complex geometries, a finite volume approach has been developed by Popescu [2]. The finite volume approach ensures that estimated fluxes at a cell face are equal and thus, satisfy the governing conservation laws of physics.

To explain the finite volume approach Popescu uses the one-dimensional linear wave equation and the geometry as given in Figure 5:

$$\frac{\partial u}{\partial t} + \frac{\partial u}{\partial x} = 0. \tag{40}$$

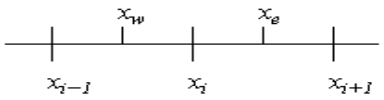

Figure 5: Cell centered grid with control volume $[x_w, x_e]$.

Integration over a cell gives:

$$\overline{\frac{\partial u}{\partial t}}\Delta x + u|_w^e = \overline{\frac{\partial u}{\partial t}}\Delta x + u_e - u_w = 0, \tag{41}$$

where $\overline{\frac{\partial u}{\partial t}}$ is an average value over a control volume.

With the finite volume approach $\frac{\partial u}{\partial x}$ is associated with $u_e - u_w$. The finite difference DRP scheme (4^{th} order, seven point stencil) looks like: $\left(\frac{du}{dx}\right)_l \simeq \frac{1}{\Delta x}\sum_{j=-3}^{3} a_j u_{l+j}$. Now u_e and u_w are approximated with their neighboring nodes:

$$\begin{aligned} u_e &= \beta_1 u_{i-2} + \beta_2 u_{i-1} + \beta_3 u_i + \beta_4 u_{i+1} + \beta_5 u_{i+2} + \beta_6 u_{i+3}, \\ u_w &= \beta_1 u_{i-3} + \beta_2 u_{i-2} + \beta_3 u_{i-1} + \beta_4 u_i + \beta_5 u_{i+1} + \beta_6 u_{i+2}. \end{aligned} \tag{42}$$

By imposing that u at the same location has the same value as in the finite differences approach, $\sum_{j=-3}^{3} a_j u_{i+j} = u_e - u_w$, the values of β_k are determined by solving the following 7 expressions:

$$\begin{aligned} -\beta_1 &= a_{-3}, \\ (\beta_1 - \beta_2) &= a_{-2}, \\ (\beta_2 - \beta_3) &= a_{-1}, \\ (\beta_3 - \beta_4) &= 0, \\ (\beta_4 - \beta 5) &= a_1, \\ (\beta_5 - \beta_6) &= a_2, \\ \beta_6 &= a_3. \end{aligned} \tag{43}$$

This procedure can easily be extended to higher dimensional problems.

2.2.3 Time Integration

For time integration Tam [1] uses an explicit multistep method with time step Δt. Suppose there is an unknown vector $u(t)$ and the solution $u(t)$ is known up to $t = n\Delta t$, then the 4-level finite differences time integration is given as follows:

$$u^{(n+1)} - u^{(n)} \simeq \Delta t \sum_{j=0}^{3} b_j \left(\frac{du}{dt}\right)^{(n-j)}. \tag{44}$$

Again a Taylor expansion is used to ensure that the scheme is 3^{rd} order in time:

$$\begin{gathered}(u^{(n)} + \Delta t \tfrac{du^{(n)}}{dt} + \tfrac{\Delta t^2}{2}\tfrac{d^2u^{(n)}}{dt^2} + \tfrac{\Delta t^3}{6}\tfrac{d^3u^{(n)}}{dt^3} + ...) - u^{(n)} \simeq \\ \Delta t \sum_{j=0}^{3} b_j \left(\tfrac{du^{(n)}}{dt} - \Delta t \tfrac{d^2u^{(n)}}{dt^2} + \tfrac{\Delta t^2}{2}\tfrac{d^3u^{(n)}}{dt^3} + ...\right).\end{gathered} \tag{45}$$

This gives three equations for four unknowns, so there is one free parameter, say b_0, with the following relations:

$$b_1 = -3b_0 + \frac{53}{12}, \qquad b_2 = 3b_0 - \frac{16}{3}, \qquad b_3 = -b_0 + \frac{23}{12}. \tag{46}$$

To determine b_0 Tam [1] uses Laplace transforms, like Fourier transforms in the space discretization, which are defined below:

$$\widehat{f}(\omega) = \frac{1}{2\pi}\int_0^\infty f(x)e^{i\omega x}dx, \tag{47}$$

and its inverse:

$$f(x) = \int_\Gamma \widehat{f}(\omega)e^{-i\omega x}d\alpha. \tag{48}$$

This leads to the derivative and shift theorems:

$$\begin{gathered}\widehat{\tfrac{\partial f}{\partial x}(x)} = -i\omega\widehat{f}(\omega), \\ \widehat{f(x+\lambda)} = e^{-i\omega\lambda}\widehat{f}(\omega).\end{gathered} \tag{49}$$

Applying this to the continuous generalization of (44) the following is determined:

$$(e^{-i\omega\Delta t} - 1)\widehat{u}^{(n)} = \Delta t \sum_{j=0}^{3} b_j e^{ij\omega\Delta t}\left(\widehat{\frac{\partial u}{\partial t}}\right)^{(n)} = -i\omega\Delta t \sum_{j=0}^{3} b_j e^{ij\omega\Delta t}\widehat{u}^{(n)}. \tag{50}$$

Thus, ω of the scheme is: $\overline{\omega} = \dfrac{i(e^{-i\omega\Delta t}-1)}{\Delta t \sum_{j=0}^{3} b_j e^{ij\omega\Delta t}}$.

To optimize the time integration scheme, the weighted error E is optimized:

$$E = \int_{-\zeta}^{\zeta} \left[\sigma(\mathrm{Re}(\overline{\omega}\Delta t - \omega\Delta t))^2 + (1-\sigma)\,\mathrm{Im}(\overline{\omega}\Delta t - \omega\Delta t))^2\right] d(\omega\Delta t). \qquad (51)$$

The value of b_0 can be determined by setting: $\frac{\partial E}{\partial b_0} = 0$.

The weight σ can be chosen to emphasize the real or imaginary part. This has the effect of better wave propagation characteristic (real part) or better dissipative characteristics (imaginary part). Tam [1] chooses $\sigma = 0.36$, which appears to be a good balance between real and imaginary part. With $\varsigma = \frac{1}{2}$ the values of b_j become [1]:

$$b_0 = 2.30256,\ b_1 = -2.49100,\ b_2 = 1.57434,\ b_3 = -0.38589.$$

The relation between $\overline{\omega}\Delta t$ and $\omega\Delta t$ is not one-to-one. For every $\overline{\omega}\Delta t$ there are four values of $\omega\Delta t$. To clarify this $\overline{\omega}$ is considered.

$$\overline{\omega} = \frac{i(e^{-i\omega\Delta t}-1)}{\Delta t \sum_{j=0}^{3} b_j e^{ij\omega\Delta t}} \qquad \Leftrightarrow \qquad \sum_{j=0}^{3} b_j e^{ij\omega\Delta t} = \frac{i(e^{-i\omega\Delta t}-1)}{\overline{\omega}\Delta t}$$

$$\Leftrightarrow \qquad \sum_{j=0}^{3} b_j e^{i(j+1)\omega\Delta t} = \frac{i(1-e^{i\omega\Delta t})}{\overline{\omega}\Delta t} \qquad \Leftrightarrow$$

$$\Leftrightarrow \qquad \sum_{j=0}^{3} b_j \left(e^{i\omega\Delta t}\right)^{j+1} + \frac{i}{\overline{\omega}\Delta t} e^{i\omega\Delta t} - \frac{i}{\overline{\omega}\Delta t} = 0.$$

By setting $z = e^{i\omega\Delta t}$ the following polynomial is obtained:

$$b_3 z^4 + b_2 z^3 + b_1 z^2 + (b_0 + \frac{i}{\overline{\omega}\Delta t})z - \frac{i}{\overline{\omega}\Delta t} = 0. \qquad (52)$$

Now, it is obvious that there are four values of $\omega\Delta t$ for every value of $\overline{\omega}\Delta t$.

This introduces spurious numerical solutions. From Figure 6 [1] it appears that:

1. There is one curve which has nearly zero imaginary part for $\overline{\omega}\Delta t < 0.6$.
2. There is a spurious curve which has negative imaginary part only for $\overline{\omega}\Delta t < 0.4$.
3. The two other curves have negative imaginary parts.

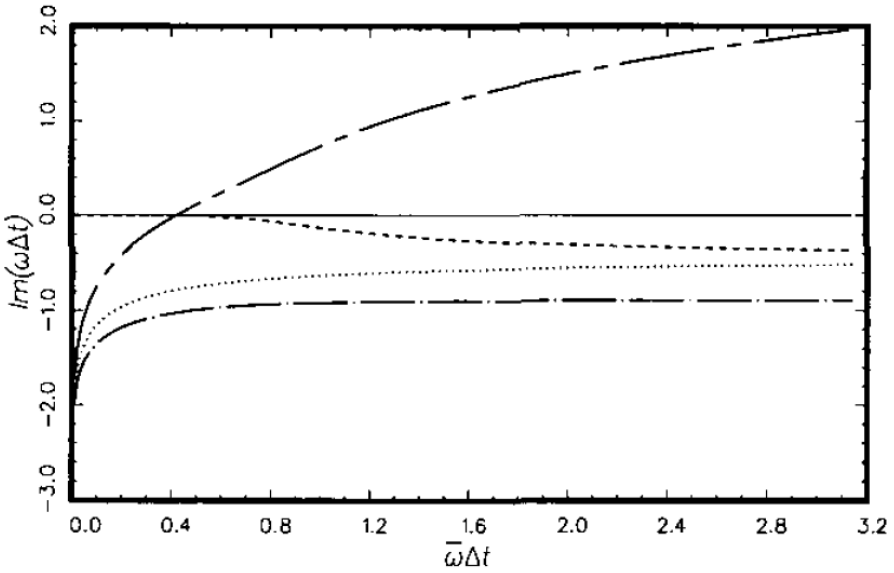

Figure 6: $\mathrm{Im}(\omega\Delta t)$ versus $\omega\Delta t$. The four roots and the ideal $\mathrm{Im}(\omega\Delta t) = 0$.

Tam [1] showed that for numerically stable results $\mathrm{Im}(\omega\Delta t) \leq 0$, so $\overline{\omega}\Delta t < 0.4$, is needed. With this condition all roots, especially the spurious, are damped out.

2.2.4 Stability

Popescu and Shyy [3] have investigated the stability of the DRP scheme for the linear wave equation, which is shown below. Tam [1] has investigated it for the linear Euler equations. The Fourier-Laplace transformation of the linear wave equation, $\frac{\partial u}{\partial t} + c\frac{\partial u}{\partial x} = 0$, is:

$$-i\overline{\omega}\widetilde{u} = -ci\overline{\alpha}\widetilde{u} \qquad \Leftrightarrow \qquad \overline{\omega}\Delta t = c\overline{\alpha}\Delta t \qquad \Leftrightarrow \qquad \overline{\omega}\Delta t = \tfrac{c\Delta t}{\Delta x}\overline{\alpha}\Delta x.$$

Tam [1] showed that $\overline{\omega}\Delta t < 0.4$ for numerical stability and that $\overline{\omega}\Delta t < 0.19$ is required for negligible numerical dissipation. Furthermore, Popescu and Shyy [3] showed that $\overline{\alpha}\Delta x < 0.9$ is required to obtain a good numerical accuracy ($\frac{d\overline{\alpha}}{d\alpha} < 1.02$). These results lead to the following condition:

$$\overline{\omega}\Delta t = \tfrac{c\Delta t}{\Delta x}0.9 = 0.9\nu \leq 0.19 \qquad \Rightarrow \qquad \nu \leq 0.211,$$

with $\nu = c\frac{\Delta t}{\Delta x}$ the CFL-number.

Now the stability condition has been obtained.

The final DRP scheme with 7-point in space (4^{th} order) and 4-point in time (3^{rd} order) for the linear wave equation is:

$$\frac{u_l^{(n+1)} - u_l^{(n)}}{\Delta t} + \frac{c}{\Delta x}\sum_{j=0}^{3} b_j \sum_{k=-3}^{3} a_k u_{l+k}^{(n-j)} = 0. \tag{53}$$

2.3 Optimized Prefactored Compact Scheme

The OPC scheme is based on prefactored compact schemes, which require very small stencil support. The prefactor procedure splits the implicit central scheme into a forward and backward operator. The compact schemes have small stencils, which implies that the specification of the boundaries is simplified, because no additional conditions have to be proposed. Another advantage of the OPC scheme is that it has the same order of accuracy with a smaller stencil than other schemes.

2.3.1 Finite Difference approach

Let us introduce first the compact scheme:

$$\begin{gathered}\beta(D_{i-2}+D_{i+2})+\eta(D_{i-1}+D_{i+1})+D_i \simeq \\ \frac{a}{2\Delta x}(u_{i+1}-u_{i-1})+\frac{b}{4\Delta x}(u_{i+2}-u_{i-2})+\frac{c}{6\Delta x}(u_{i+3}-u_{i-3}).\end{gathered} \tag{54}$$

where D_i is the spatial derivative of u in the point x_i.
A Taylor series expansion is showed below:

$$\begin{gathered}2\beta(\frac{\partial u_i}{\partial x}+\frac{(2\Delta x)^2}{2}\frac{\partial^3 u_i}{\partial x^3}+\frac{(2\Delta x)^4}{4!}\frac{\partial^5 u_i}{\partial x^5}+...)+ \\ 2\eta(\frac{\partial u_i}{\partial x}+\frac{\Delta x^2}{2}\frac{\partial^3 u_i}{\partial x^3}+\frac{\Delta x^4}{4!}\frac{\partial^5 u_i}{\partial x^5}+...)+\frac{\partial u_i}{\partial x}\simeq \\ 2\frac{a}{2\Delta x}(\frac{\partial u_i}{\partial x}\Delta x+\frac{\Delta x^3}{3!}\frac{\partial^3 u_i}{\partial x^3}+\frac{\Delta x^5}{5!}\frac{\partial^5 u_i}{\partial x^5}+...)+ \\ 2\frac{b}{4\Delta x}(\frac{\partial u_i}{\partial x}(2\Delta x)+\frac{(2\Delta x)^3}{3!}\frac{\partial^3 u_i}{\partial x^3}+\frac{(2\Delta x)^5}{5!}\frac{\partial^5 u_i}{\partial x^5}+...)+ \\ \frac{c}{6\Delta x}(\frac{\partial u_i}{\partial x}(3\Delta x)+\frac{(3\Delta x)^3}{3!}\frac{\partial^3 u_i}{\partial x^3}+\frac{(3\Delta x)^5}{5!}\frac{\partial^5 u_i}{\partial x^5}+...).\end{gathered} \tag{55}$$

After matching coefficients the following relations can be obtained [4]:
Second order:

$$a+b+c=1+2\eta+2\beta, \tag{56}$$

Fourth order:

$$a+2^2b+3^2c=2\frac{3!}{2!}(\eta+2^2\beta), \tag{57}$$

Sixth order:

$$a+2^4b+3^4c=2\frac{5!}{4!}(\eta+2^4\beta), \tag{58}$$

etc.
Only for tenth order all coefficients are unique.

Also the numerical wavenumber of (54) can be determined by the Fourier transform and its shift and derivative theorems:

$$\begin{gathered}\beta(e^{-i\alpha 2\Delta x}+e^{i\alpha 2\Delta x})i\alpha\widetilde{u}+\eta(e^{-i\alpha\Delta x}+e^{i\alpha\Delta x})i\alpha\widetilde{u}+i\alpha\widetilde{u}\simeq \\ \frac{a}{2\Delta x}(e^{i\alpha\Delta x}-e^{-i\alpha\Delta x})\widetilde{u}+\frac{b}{4\Delta x}(e^{i\alpha 2\Delta x}-e^{-i\alpha 2\Delta x})\widetilde{u}+ \\ \frac{c}{6\Delta x}(e^{i\alpha 3\Delta x}-e^{-i\alpha 3\Delta x})\widetilde{u},\end{gathered} \tag{59}$$

$$(2\beta\cos(2\alpha\Delta x)+2\eta\cos(\alpha\Delta x)+1)i\alpha\widetilde{u}\simeq$$
$$(\tfrac{a}{\Delta x}\sin(\alpha\Delta x)+\tfrac{b}{2\Delta x}\sin(2\alpha\Delta x)+\tfrac{c}{3\Delta x}\sin(3\alpha\Delta x))i\widetilde{u}. \tag{60}$$

Hence, the (real) numerical wavenumber is given by:

$$\overline{\alpha}\Delta x=\frac{a\sin(\alpha\Delta x)+\frac{b}{2}\sin(2\alpha\Delta x)+\frac{c}{3}\sin(3\alpha\Delta x)}{2\beta\cos(2\alpha\Delta x)+2\eta\cos(\alpha\Delta x)+1}. \tag{61}$$

The prefactored compact scheme is defined using a forward and backward operator [4]. This leads to reduced, upper and lower bidiagonal, matrices, which is advantageous when these have to be inverted (This procedure is described in the last part of this section).

$$D_i=\frac{1}{2}(D_i^B+D_i^F), \tag{62}$$

which are defined by:

$$\beta_F D_i^F+\eta_F D_{i+1}^F\simeq\frac{1}{\Delta x}[a_F u_{i+2}+b_F u_{i+1}+c_F u_i+d_F u_{i-1}+e_F u_{i-2}], \tag{63}$$

$$\gamma_B D_{i-1}^B+\beta_B D_i^B\simeq\frac{1}{\Delta x}[a_B u_{i+2}+b_B u_{i+1}+c_B u_i+d_B u_{i-1}+e_B u_{i-2}]. \tag{64}$$

Again Fourier transforms determine the numerical wavenumer of these operators, which have a real and imaginary part.

Forward stencil:

$$\begin{aligned}\mathrm{Re}(\overline{\alpha}_F\Delta x)=\quad&\tfrac{(a_F\eta_F+b_F\beta_F-c_F\eta_F-d_F\beta_F)\sin(\alpha\Delta x)}{\eta_F^2+\beta_F^2+2\eta_F\beta_F\cos(\alpha\Delta x)}+\\&\tfrac{(a_F\beta_F-d_F\eta_F-e_F\beta_F)\sin(2\alpha\Delta x)-e_F\eta_F\sin(3\alpha\Delta x)}{\eta_F^2+\beta_F^2+2\eta_F\beta_F\cos(\alpha\Delta x)},\end{aligned} \tag{65}$$

$$\begin{aligned}\mathrm{Im}(\overline{\alpha}_F\Delta x)=\quad&\tfrac{-(b_F\eta_F+c_F\beta_F)-(a_F\eta_F+b_F\beta_F+c_F\eta_F+d_F\beta_F)\cos(\alpha\Delta x)}{\eta_F^2+\beta_F^2+2\eta_F\beta_F\cos(\alpha\Delta x)}+\\&\tfrac{-(a_F\beta_F+d_F\eta_F+e_F\beta_F)\cos(2\alpha\Delta x)-e_F\eta_F\cos(3\alpha\Delta x)}{\eta_F^2+\beta_F^2+2\eta_F\beta_F\cos(\alpha\Delta x)}.\end{aligned} \tag{66}$$

Backward stencil:

$$\begin{aligned}\mathrm{Re}(\overline{\alpha}_B\Delta x)=\quad&\tfrac{(b_B\beta_B+c_B\gamma_B-d_B\beta_B-e_B\gamma_B)\sin(\alpha\Delta x)}{\gamma_B^2+\beta_B^2+2\gamma_B\beta_B\cos(\alpha\Delta x)}+\\&\tfrac{(a_B\beta_B+b_B\gamma_B-e_B\beta_B)\sin(2\alpha\Delta x)+a_B\gamma_B\sin(3\alpha\Delta x)}{\gamma_B^2+\beta_B^2+2\gamma_B\beta_B\cos(\alpha\Delta x)},\end{aligned} \tag{67}$$

$$\begin{aligned}\mathrm{Im}(\overline{\alpha}_B\Delta x)=\quad&\tfrac{-(c_B\beta_B+d_B\gamma_B)-(b_B\beta_B+c_B\gamma_B+d_B\beta_B+e_B\gamma_B)\cos(\alpha\Delta x)}{\gamma_B^2+\beta_B^2+2\gamma_B\beta_B\cos(\alpha\Delta x)}+\\&\tfrac{-(a_B\beta_B+b_B\gamma_B+e_B\beta_B)\cos(2\alpha\Delta x)-a_B\gamma_B\cos(3\alpha\Delta x)}{\gamma_B^2+\beta_B^2+2\gamma_B\beta_B\cos(\alpha\Delta x)}.\end{aligned} \tag{68}$$

The real parts represent the dispersion relation and the imaginary parts the dissipation.

To be equivalent with the original compact scheme Hixon and Turkel [5] defined several conditions:

1. The imaginary parts of the forward and backward wavenumbers have to be equal but of opposite sign.

2. The real parts have to be equal and also equal to the wavenumber of the compact scheme.

To satisfy the first condition the following is required:

$$\begin{gathered} \beta_B = \beta_F, \qquad \gamma_B = \eta_F, \\ a_B = -e_F, \qquad b_B = -d_F, \qquad c_B = -c_F, \qquad d_B = -b_F, \qquad e_B = -a_F. \end{gathered} \tag{69}$$

To satisfy the second condition and supplementary relation $a_F + b_F + c_F + d_F + e_F = 0$, to ensure that when gradients are zero the computed gradients are also zero, the coefficients are known as a function of a, b, c, β and η, which are not completely determined yet in case of lower order accuracy than 10^{th} order.

Now the stencil has to be optimized. The optimize technique is applied to the original compact scheme. Again an error E is defined to measure the difference between the wavenumber and the numerical wavenumber:

$$E = \int_0^{r\pi} (\alpha\Delta x - \overline{\alpha}\Delta x) W(\alpha\Delta x) d(\alpha\Delta x), \tag{70}$$

where $W(\alpha\Delta x)$ is a weigth function, which makes the expression analytically integrable, and r defines the optimized range. Kim and Lee [6] chose the function $W(\alpha\Delta x) = [2\beta\cos(2\alpha\Delta x) + 2\eta\cos(\alpha\Delta x) + 1]^2$. How much free variables are present depends on the choice of the order of accuracy. The errorfunction can be minimized by the free parameter(s) and now the problem is closed and all parameters of the compact scheme are known, which implies that also all parameters of the forward and backward schemes are known. This optimization procedure leads to 4^{th} order accuracy for a scheme with maximum 6^{th} order (6/4 OPC) with a three-point stencil and for a scheme with maximum 8^{th} order (8/4 OPC) with a five-point stencil.

Also boundary stencils have to be taken into account. For example, for a three-point stencil the forward and backward boundary stencils are explicitly defined:

$$\begin{gathered} D_1^B = \tfrac{1}{\Delta x} \sum_{j=1}^{4} s_j u_j, \qquad D_N^B = \tfrac{1}{\Delta x} \sum_{j=N-3}^{N} e_j u_j, \\ D_1^F = \tfrac{1}{\Delta x} \sum_{j=1}^{4} -e_{N+1-j} u_j, \quad D_N^F = \tfrac{1}{\Delta x} \sum_{j=N-3}^{N} -s_{N+1-j} u_j, \end{gathered} \tag{71}$$

where the coefficients s_j and e_j are determined by matching coefficients from the Taylor series expansion.

Now, the system of equations following from (63) and (64) can be written as follows:

$$[A^F] D^F = [B^F] u, \tag{72}$$

$$[A^B]D^B = [B^B]u, \tag{73}$$

where [.] are matrices.

The system of equations following from (62) can be obtained using (72) and (73):

$$D = \frac{1}{2}([A^F]^{-1}[B^F] + [A^B]^{-1}[B^B])u. \tag{74}$$

Figure 7 [2] shows $\overline{\alpha}\Delta x$ as a function of $\alpha\Delta x$ for several schemes. Also the ideal situation $\overline{\alpha}\Delta x = \alpha\Delta x$ for all $\alpha\Delta x$ is shown.

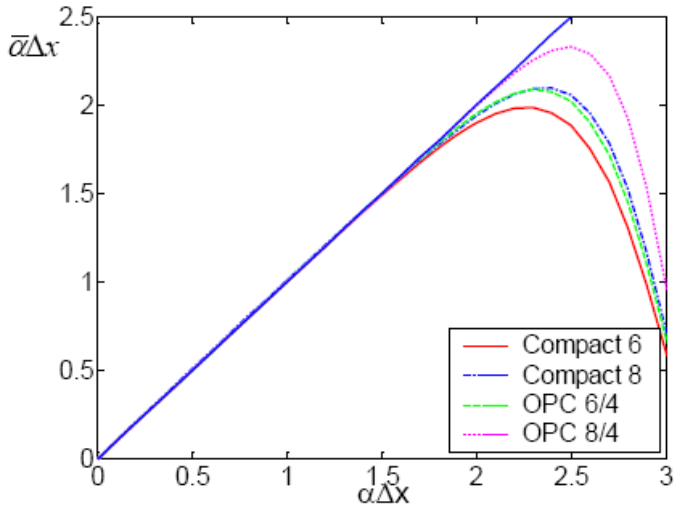

Figure 7: $\alpha\Delta x$ versus $\overline{\alpha}\Delta x$ for two OPC schemes and two compact schemes.

Like in the DRP case, it appears that $\overline{\alpha}\Delta x$ and $\alpha\Delta x$ are nearly the same up to $\alpha_c\Delta x$, which is easily determined by a simple condition, e.g. $|\alpha\Delta x - \overline{\alpha}\Delta x| < 0.001$. Also the group velocity is considered and compared with the other schemes in Figure 8 [2].

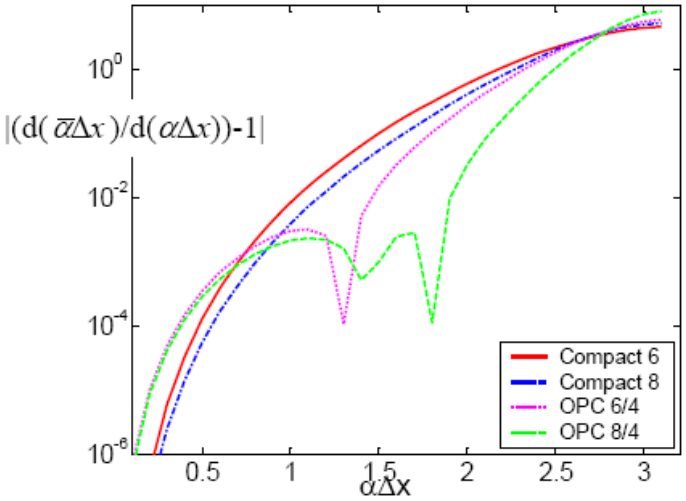

Figure 8: $\left|\frac{d(\bar{\alpha}\Delta x)}{d(\alpha\Delta x)} - 1\right|$ versus $\alpha\Delta x$ for two OPC schemes and two compact schemes.

It appears from the figures that the OPC schemes produce quite good results over a large range of wavenumbers.

2.3.2 Finite Volume approach

For the finite volume derivation of the OPC scheme Popescu [2] uses again the one-dimensional linear wave equation and the geometry as given in Figure 5.

$$\frac{\partial u}{\partial t} + \frac{\partial u}{\partial x} = 0. \tag{75}$$

Integration over a cell gives:

$$\left(\overline{\frac{\partial u}{\partial t}}\right)_i \Delta x + u_i|_w^e = \left(\overline{\frac{\partial u}{\partial t}}\right)_i \Delta x + u_i^e - u_i^w = 0, \tag{76}$$

where $\left(\overline{\frac{\partial u}{\partial t}}\right)_i$ is an average value over a control volume i.

Equations (62), (63) and (64) describe the OPC scheme and the approximations of u_e and u_w have similar forms:

$$\begin{aligned} u_i^e &= \tfrac{1}{2}(u_i^{Fe} + u_i^{Be}), \\ u_i^w &= \tfrac{1}{2}(u_i^{Fw} + u_i^{Bw}), \end{aligned} \tag{77}$$

where u_i^{Fe}, u_i^{Be}, u_i^{Fw} and u_i^{Bw} are determined from:

$$\begin{aligned} \eta u_{i+1}^{Fe} + \beta u_i^{Fe} &= b u_{i+1} - d u_i, \\ \eta u_{i+1}^{Fw} + \beta u_i^{Fw} &= b u_i - d u_{i-1}, \\ \beta u_i^{Be} + \eta u_{i-1}^{Be} &= b u_i - d u_{i+1}, \\ \beta u_i^{Bw} + \eta u_{i-1}^{Bw} &= b u_{i-1} - d u_i. \end{aligned} \tag{78}$$

Here the coefficients η, β, b and d are the same as in the finite difference approach: $\eta = \eta_F$, $\beta = \beta_F$, $b = b_F$ and $d = d_F$.

In order to solve this, explicit boundary stencils are required like (71):

$$\begin{aligned} u_1^w &= \sum_{i=1}^{3} a_i u_i, \qquad u_N^w = \sum_{i=1}^{3} r_i u_{N-i}, \\ u_1^e &= \sum_{i=1}^{3} a_i u_{i+1}, \quad u_N^e = \sum_{i=1}^{3} r_i u_{N-i+1}, \end{aligned} \tag{79}$$

all for forward and backward operators. Where the coefficients are:

$$\begin{aligned} a_1^B &= -s_1, & a_1^F &= e_N, \\ a_2^B &= -s_1 - s_2, & a_2^F &= e_N + e_{N-1}, \\ a_3^B &= -s_1 - s_2 - s_3, & a_3^F &= e_N + e_{N-1} - e_{N-2}, \\ r_1^B &= e_N, & r_1^F &= -s_1, \\ r_2^B &= e_N + e_{N-1}, & r_2^F &= -s_1 - s_2, \\ r_3^B &= e_N + e_{N-1} - e_{N-2}, & r_3^F &= -s_1 - s_2 - s_3. \end{aligned} \tag{80}$$

Now, the systems of equations can be solved like in the finite differences approach.

2.3.3 Time Integration

For time integration the modified Runge-Kutta scheme, Low Dispersion and Dissipation Runge-Kutta (LDDRK), has been developed by Hu, Hussaini and Manthey [7]. In the original Runge-Kutta scheme the coefficients are chosen such that the Taylor series coefficients match up to a certain order of accuracy. The Runge-Kutta scheme is applied to the equation:

$$\frac{du}{dt} = F(u). \tag{81}$$

Consider the original p-stage explicit Runge-Kutta scheme in the $(n+1)^{th}$ iteration:

$$\begin{aligned} K_1 &= \Delta t F(u^n), \\ &\vdots \\ K_i &= \Delta t F(u^{(i-1)}), \\ u^{(i)} &= u^n + b_i K_i, \qquad i = 1...p, \\ &\vdots \\ u^{n+1} &= u^{(p)}, \end{aligned} \tag{82}$$

where $b_p = 1$. See Appendix to note the equivalence of this notation and standard notation for linear problems.

Another way to write u^{n+1} is:

$$u^{n+1} - u^n \simeq \sum_{j=1}^{p} \prod_{l=p-j+1}^{p} b_l \Delta t^j \frac{d^j u^n}{dt^j}. \tag{83}$$

When the left hand side of this equation is expanded into a truncated Taylor series and the right hand side is written out the coefficients $\gamma_j = \prod_{l=p-j+1}^{p} b_l$ can be determined:

$$\begin{gathered} \Delta t \frac{du^n}{dt} + \frac{\Delta t^2}{2} \frac{d^2 u^n}{dt^2} + ... + \frac{\Delta t^p}{p!} \frac{d^p u^n}{dt^p} \simeq \\ b_p \Delta t \frac{du^n}{dt} + (b_p b_{p-1}) \Delta t^2 \frac{d^2 u^n}{dt^2} + ... + (b_p ... b_1) \Delta t^p \frac{d^p u^n}{dt^p}. \end{gathered} \tag{84}$$

Hence, $\gamma_j = \frac{1}{j!}$ for p^{th} order accuracy, like in the p-stage standard Runge-Kutta.

By applying Fourier transforms to (83) the numerical amplification factor r is obtained:

$$r = \frac{\widetilde{u}^{n+1}}{\widetilde{u}^n} = 1 + \sum_{j=1}^{p} \gamma_j (-i\overline{\omega}\Delta t)^j = 1 + \sum_{j=1}^{p} \gamma_j (-i\sigma)^j \,. \tag{85}$$

Also the exact amplification factor can be obtained:

$$r_{exact} = e^{-i\overline{\omega}\Delta t} = e^{-i\sigma}. \tag{86}$$

With $\gamma_j = \frac{1}{j!}$, it is easy to see that the numerical amplification factor is the truncated Taylor series of the exact amplification factor. To compare the exact and numerical amplification factor its ratio have to be obtained:

$$\frac{r}{r_{exact}} = \frac{1 + \sum_{j=1}^{p} \gamma_j (-i\sigma)^j}{e^{-i\sigma}}, \tag{87}$$

which can be rewritten as:

$$\frac{r}{r_{exact}} = |\eta| e^{-i\delta}. \tag{88}$$

In this expression $|\eta|$ represents the dissipation rate and δ represents the dispersion rate. Where the $|\eta|$ should be 1 and δ should be 0 for r and r_{exact} to be equal. Thus for accuracy's sake δ must be close to 0 and $|\eta|$ must be close to 1 and for stability's sake $|\eta| \leq 1$. To obtain this the Runge-Kutta method has to be modified to optimize the dispersion and dissipation rate. Hu, Hussiani and Manthey [7] showed that it is sufficient to minimize $|r - r_{exact}|^2$ as a function of $\overline{\omega}\Delta t$:

$$\min_{\gamma_j} \int_0^{\Gamma} \left| 1 + \sum_{j=1}^{p} \gamma_j (-i\overline{\omega}\Delta t)^j - e^{-i\overline{\omega}\Delta t} \right|^2 d(\overline{\omega}\Delta t) \,, \tag{89}$$

with a supplementary condition of $|\eta| \leq 1$ and $[0, \Gamma]$ the optimization range.

Hu, Hussiani and Manthey [7] showed that $|r - r_{exact}|^2$ is an approximation of the sum of the dispersion and dissipation errors. They also showed that minimization of this integral also preserves frequency. In Figure 9 [2] it's obvious that LDDRK has better dispersion and dissipation properties than the ordinary Runge-Kutta integration. Here L and R denote the accuracy limit and the stability limit respectively.

Also the dissipation and dispersion error of an alternating scheme can be optimized. An example of the alternating scheme 4-6-LDDRK: in the odd time steps the four stage LDDRK and the even time steps the six stage LDDRK is used. In this procedure $|r_4 r_6 - r^2_{exact}|^2$ is minimized. For alternating schemes the dissipation and dispersion error can be further reduced with the minimization and another advantage is that higher order of accuracy can be maintained. Hu, Hussiani and Manthey [7] present the coefficients of 4-6-LDDRK and 5-6-LDDRK, which are both fourth order accurate.

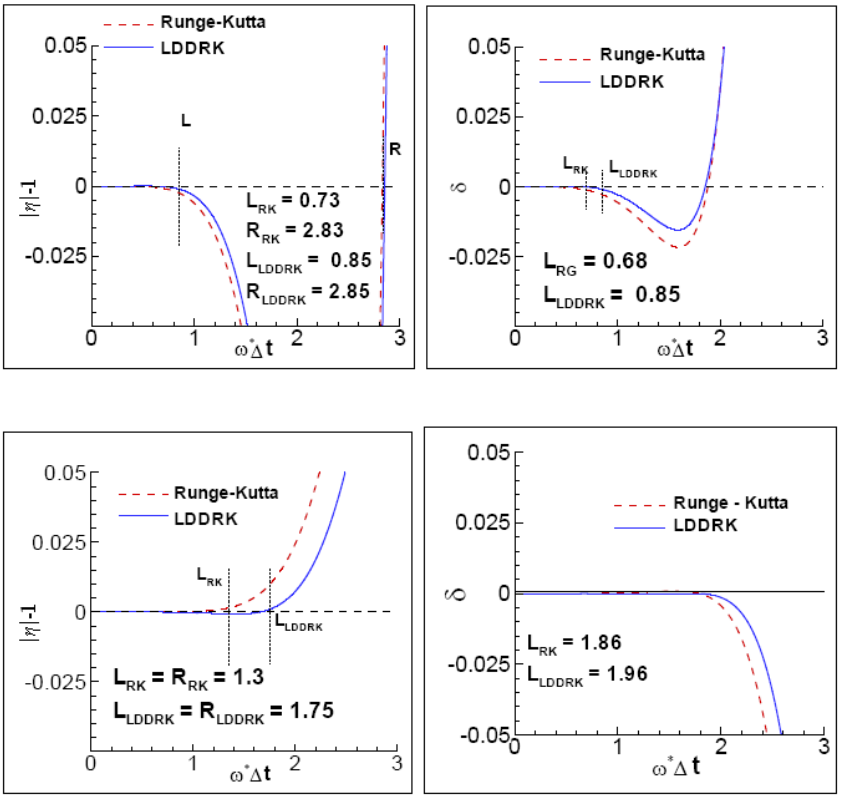

Figure 9: Dissipation and dispersion errors. Above 4 stages, below 6 stages.

Popescu [2] specifies the coefficients of the 4-6-LDDRK scheme:

1. Four stages:
   $b_1 = \frac{1}{4}, \qquad b_2 = \frac{1}{3}, \qquad b_3 = \frac{1}{2}.$
2. Six stages:
   $b_1 = 0.17667, \qquad b_2 = 0.38904, \qquad b_3 = \frac{1}{4}, \qquad b_4 = \frac{1}{3}, \qquad b_5 = \frac{1}{2}.$

2.3.4 Stability

For the investigation of the stability of the OPC scheme the linear wave equation is used, which is shown below. The Fourier-Laplace transformation of the linear wave equation, $\frac{\partial u}{\partial t} + c\frac{\partial u}{\partial x} = 0$, is:

$$-i\overline{\omega}\widetilde{u} = -ci\overline{\alpha}\widetilde{u} \qquad \Leftrightarrow \qquad \overline{\omega}\Delta t = c\overline{\alpha}\Delta t \qquad \Leftrightarrow \qquad \overline{\omega}\Delta t = \tfrac{c\Delta t}{\Delta x}\overline{\alpha}\Delta x.$$

Popescu [2] showed that $\overline{\alpha}\Delta x < 1.4$ is required and that $\overline{\alpha}\Delta x < 1.9$ is required for respectively 6/4-scheme and 8/4-scheme for low dispersion error. Criterion $\left|\frac{d(\overline{\alpha}\Delta x)}{d(\alpha\Delta x)} - 1\right| < 3 \cdot 10^{-3}$ is used to obtain these requirements. This is also illustrated in Figure 7 and Figure 8. Popescu [2] showed that for numerical stability of the 4-6-LDDRK $\overline{\omega}\Delta t < 2.52$ is required. For accuracy's sake this requirement is replaced by $\overline{\omega}\Delta t < 1.64$ which also satisfies the requirement of negligible numerical dissipation. These results lead to the following condition:

$$\overline{\omega}\Delta t = \tfrac{c\Delta t}{\Delta x}1.4 = 1.4\nu \leq 1.64 \qquad \Rightarrow \qquad \nu \leq 1.17,$$

with $\nu = c\frac{\Delta t}{\Delta x}$ the CFL-number.

Now the stability condition has been obtained for the 6/4-OPC scheme in combination with the 4-6-LDDRK scheme.

2.4 Cut-Cell Method

In general there are two approaches to generate a grid.

1. A boundary conforming grid: the grid lines match with the boundary
2. A boundary non-conforming grid, the grid lines do not match or intersect the boundary

Often the first option results in curvilinear grids, for which numerical schemes are harder to implement due to the irregular cells. With the second option often a Cartesian grid is used, for which special treatment for each boundary cell is required. A great advantage of this Cartesian grid is the easy implementation for the interior domain. For the implementation of the boundaries the cut-cell technique is used. The standard second order cut-cell method is described below as an introduction for the cut-cell method for acoustic problems which is described later.

2.4.1 Ordinary Second Order Cut-Cell Method

The basic idea of the cut-cell method is to rearrange the control volumes, which are in vicinity of the boundaries, to create cells that conform the boundaries. Cells are cut off according to the boundary and become an independent cell or are merged with another (cut) cell. Cut cells are merged with others if the cell area is less than a minimum acceptable cell area $S_{\min}$. Otherwise, it could be independent. So, this procedure produces new irregular shaped boundary cells. In a finite volume approach the fluxes across the faces of the cells are approximated by:

$$\oint f \cdot n ds \approx \sum_{i=1}^{k} f_i n_i, \tag{90}$$

where flux f contains both the convective and the diffusive flux, resulting from a differential equation for ϕ. To compute the fluxes on the faces the midpoint rule is used which means that the fluxes are evaluated at the center of the faces.

For further explanation of the cut-cell method the geometry as in Figure 10 is used.

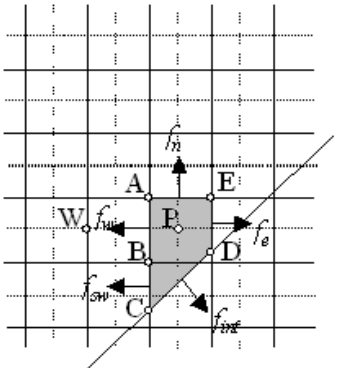

Figure 10: Two cut cells, $ABDE$ and BCD, are merged into a new cell $ABCDE$.

The approximation of the flux on a face is split into an approximation of the flux on a cut face and an approximation of the flux on a regular face. For example, the flux on face AC in Figure 10 is split into a flux f_w on regular face AB and a flux f_{sw} on cut face BC, which results in:

$$\int_{AC} f dy = \int_{AB} f dy + \int_{BC} f dy. \tag{91}$$

This integral can be approximated by:

$$\int_{AC} f dy \approx f_w(y_A - y_B) + f_{sw}(y_B - y_C). \tag{92}$$

In this case a second order approximation of f_w can be made just by linear interpolation of neighboring nodes P and W. For example if f_w requires a value for ϕ, this can be interpolated: $\phi_w = \lambda\phi_W + (1-\lambda)\phi_P$. If f_w requires the derivative of ϕ, this can be handled by a second order finite difference approximation.

This can't be done for the fluxes f_{sw} and f_e, because of the absence of neighboring nodes due to the boundary. The approximation for f_{sw} is shown below, whereas f_e can be done in the same way. These fluxes can be approximated by making an interpolation polynomial. To make a second order approximation an interpolation polynomial is made that is linear in x and quadratic in y:

$$\phi(x,y) = c_1xy^2 + c_2y^2 + c_3xy + c_4y + c_5x + c_6. \tag{93}$$

So,

$$\frac{\partial\phi}{\partial x} = c_1y^2 + c_3y + c_5. \tag{94}$$

This polynomial has six unknown coefficients. In order to solve these coefficients six neighboring points are needed. The trapezoidal region defined for this is shown in Figure 11.

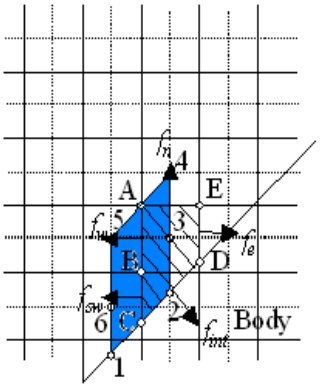

Figure 11: Cut cell $ABCDE$ (lined) and the trapezoidel region 123456 (blue) for the interpolation polynomial.

Substituting these six points into the interpolation polynomial leads to the following system:

$$\begin{bmatrix} \phi_1 \\ \phi_2 \\ \vdots \\ \phi_6 \end{bmatrix} = \begin{bmatrix} x_1y_1^2 & y_1^2 & x_1y_1 & y_1 & x_1 & 1 \\ x_2y_2^2 & y_2^2 & x_2y_2 & y_2 & x_2 & 1 \\ \vdots & \vdots & \vdots & \vdots & \vdots & \vdots \\ x_6y_6^2 & y_6^2 & x_6y_6 & y_6 & x_6 & 1 \end{bmatrix} \begin{bmatrix} c_1 \\ c_2 \\ \vdots \\ c_6 \end{bmatrix}. \tag{95}$$

This system is easily inverted, which gives c_1,..., c_6 in terms of ϕ_1,..., ϕ_6. Now, ϕ_{sw} and $\frac{\partial \phi_{sw}}{\partial x}$ are determined in terms of the neighboring nodes ϕ_1,..., ϕ_6 by substituting c_1,..., c_6, x_{sw} and y_{sw} into the interpolation polynomial.

In a similar way f_e can be determined. Also north and south faces, which are cut, are treated in this way. The only difference is that the interpolation polynomial is linear in y and quadratic in x.

Now, f_{int} on face CD has to be calculated. Since f_{int} is on the boundary, given boundary conditions could be implemented. When Dirichlet conditions are given this can directly be implemented. Then only $\frac{\partial \phi_{int}}{\partial n}$ is needed to approximate, when present in f_{int}. When Neumann conditions are given, only ϕ_{int} is needed to approximate. Below the description of the approximation for $\frac{\partial \phi_{int}}{\partial n}$:

$$\frac{\partial \phi}{\partial n} = \frac{\partial \phi}{\partial x} n_x + \frac{\partial \phi}{\partial y} n_y, \tag{96}$$

where n_x and n_y are the components of the unit normal vector of face CD,

which are known. From Figure 11 it appears that f_{int} lies on node 2. This implies that node 3, 4 and "4_n" (north neighboring node of 4) are its neighboring nodes in y-direction. So for the approximation of $\frac{\partial \phi}{\partial y}$ the interpolation polynomial is only quadratic in y:

$$\phi(y) = c_1 y^2 + c_2 y + c_3, \tag{97}$$

for which the resulting system is easily solved. The approximation of $\frac{\partial \phi_{int}}{\partial y}$ is written as $\frac{\partial \phi_{int}}{\partial y} \approx 2c_1 y_{int} + c_2$.

To approximate $\frac{\partial \phi_{int}}{\partial x}$ the procedure is similar to the procedure used for the approximation of $\frac{\partial \phi_{sw}}{\partial x}$.

All fluxes have been determined now.

2.4.2 Cut-Cell Method for CAA Approach

In order to preserve the order of accuracy as developed in the DRP or OPC schemes the same order of accuracy is needed for the boundary implementation. To explain the adapted procedure for the CAA approach, again the geometry as in Figure 10 is used. Also the finite volume technique is used and gives the integral approximations as described in the ordinary cut-cell procedure. Only difference is the approximations of the fluxes.

Now f_w can be approximated by a given boundary stencil of the DRP or OPC scheme. For the OPC scheme this is for example (71) and for the DRP scheme ghostpoints have to be introduced. In the ordinary cut-cell procedure central differences and interpolation are used to approximate f_w.

To find a fourth order approximation of f_{sw} an interpolation polynomial is used. To make this approximation fourth order this polynomial is third order in x and fourth order in y:

$$\phi(x, y) = \sum_{i=0}^{4} \sum_{j=0}^{3} c_{ij} x^j y^i. \tag{98}$$

This polynomial has 20 unknown coefficients. Thus, 20 points are needed to determine these coefficients in terms of ϕ_1,..., ϕ_{20}. The trapezoidel region with points 1,..., 20 are shown in Figure 12. This results in a similar system as in the ordinary case. The only difference is that the system is now $\phi = [A]c$, with ϕ and c twenty-dimensional vectors and $[A]$ a 20×20 matrix, which is easily inverted.

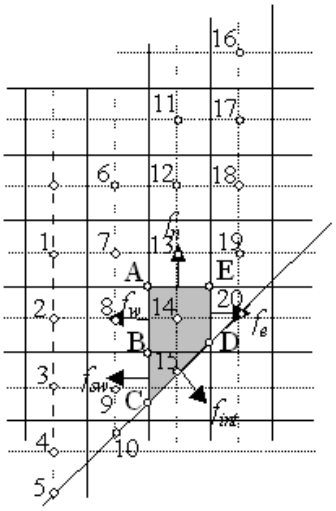

Figure 12: The cut cell $ABCDE$ and the trapezoidal $1 \cdots 20$ to approximate f_{sw}.

Also the approximation of f_e can be done with this procedure as well as north and south fluxes of this kind.

The approximation of f_{int} in this case is also similar to the approximation in the ordinary case. Again the approximation of the normal derivative is explained:

$$\frac{\partial \phi}{\partial n} = \frac{\partial \phi}{\partial x} n_x + \frac{\partial \phi}{\partial y} n_y, \tag{99}$$

where $\frac{\partial \phi_{int}}{\partial x}$ can be approximated by a interpolation polynomial that is third order in x and fourth order in y, like f_{sw} has been approximated, and $\frac{\partial \phi_{int}}{\partial y}$ can be approximated by a polynomial that is fourth order in y along the vertical line 14, 13, 12 , 11 and "11_n":

$$\phi(y) = c_1 y^4 + c_2 y^3 + c_3 y^2 + c_4 y + c_5, \tag{100}$$

with derivative:

$$\frac{\partial \phi}{\partial y} = 4c_1 y^3 + 3c_2 y^2 + 2c_3 y + c_4. \tag{101}$$

Substituting these 5 points in (100) leads to a small system, which is easily solved.

All fluxes have been determined with this cut-cell method. The procedure for acoustic problems is similar to that for ordinary problems, the only extension is higher order interpolation polynomials.

3 Conclusions and Future Work

3.1 Introduction

In the previous chapters several numerical methods have been presented. The DRP and OPC schemes have been assessed by Popescu, Shyy and Garbey [12] for both finite difference and finite volume approach. Several testcases, such as linear and nonlinear wave equation with and without viscosity, were used to compare the performances of the schemes. It turned out that the finite volume versions of the schemes produce much better results than their finite difference versions in case of nonlinearity and high gradients. For the linear wave equation the DRP and OPC schemes perform with similar order of accuracy. However, the magnitude of the error is lower for the OPC schemes.

The problem, posed in Section 1.3, tests the cut-cell procedure and the outflow boundary condition in combination with a spatial discretization and time integration method. Before the numerical simulation of this problem, Popescu, Shyy and Tai [11] first test two similar problems. First, a simulation of the radiation, generated by the baffled piston without reflection by a solid wall is done, in order to test the outflow boundary conditions and the numerical schemes. In this problem the boundary conditions for the east, west and upper bound of the computational domain are all outflow conditions. Second, a simulation of an acoustic pulse, reflected by a solid wall is done, in order to test the cut-cell procedure. This problem has the same geometry and boundary conditions as the problem, posed in Section 1.3. After these simulations, the simulation of the problem in Section 1.3 is done, which means a test for all aspects.

A challenge of this problem is to handle the discontinuity at the front of the wave. Despite the problem can be solved by taking the solid wall parallel to the grid lines, the wall is deliberately placed at an angle, in order to evaluate the performance of the cut-cell method.

3.2 Results

For the spatial discretization of the linearized Euler equations (28) Popescu, Shyy and Tai [11] use the finite volume version of the 6/4 OPC scheme. A uniform grid is used with $\Delta x = \Delta y = 0.05$ and $CFL = c_0 \frac{\Delta t}{\Delta x} = 0.5$ to determine the time step. For time integration the 4-6-LDDRK method with the time step, that just has been defined, is used.

The initial condition (29) and boundary condition (30a) are easily implemented.

In vicinity of the solid wall the cut-cell procedure is used. For the implementation of boundary condition (30b) Figure 13 [11] is used to clarify the procedure.

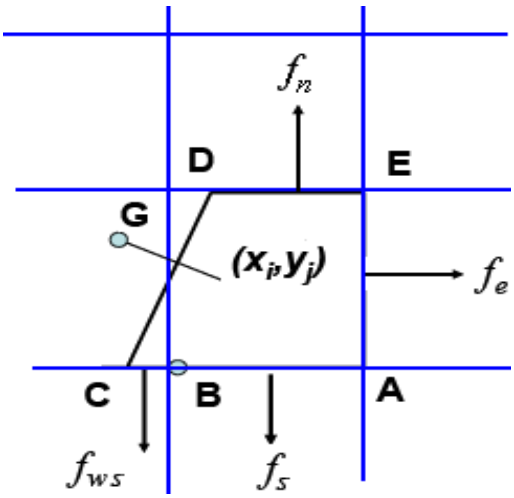

Figure 13: Geometry in vicinity of the solid wall with cut cell $ABCDE$.

The interpolation polynomials as described in Section 2.4.2 are fourth order in y and third order in x. For this problem the interpolation polynomials are fourth order in x and y. The fluxes f_{ws} and f_n are approximated with these polynomials. For the fluxes f_s and f_e the boundary stencils of the OPC scheme can be used. For the flux on face CD a virtual point G is defined. Point (x_i, y_j) is the mass center of the boundary cell and G is the symmetrical opposite of this mass center. Then $\boldsymbol{u}_{CD}$ and p_{CD} are defined as follows:

$$\begin{aligned} \boldsymbol{u}_{CD} &= \tfrac{\boldsymbol{u}_{ij}+\boldsymbol{u}_G}{2}, \qquad \text{with } \boldsymbol{u}_G = \boldsymbol{u}_{ij} - 2(\boldsymbol{u}_{ij}\cdot\boldsymbol{n})\boldsymbol{n}. \\ p_{CD} &= \tfrac{p_{ij}+p_G}{2}, \qquad \text{with } p_G = p_{ij}. \end{aligned}$$

After some mathematical manipulation it appears that boundary condition (30b) holds.

The modelling of the outflow boundary conditions (30c) are based on the outflow boundary conditions of Tam [1]:

$$\begin{aligned} \tfrac{\partial p}{\partial t} + \tfrac{\partial p}{\partial x}\cos(\theta) + \tfrac{\partial p}{\partial y}\sin(\theta) + \tfrac{p}{2r} = 0, \\ \tfrac{\partial \boldsymbol{u}}{\partial t} + \nabla p = 0, \end{aligned} \tag{102}$$

where r is the distance from the boundary point to the center of the piston and θ the angular coordinate.

In Figure 14 the contour plots of the pressure of the numerical results of this problem are presented [11]. The angle of the wall is $\beta = 63^o$.

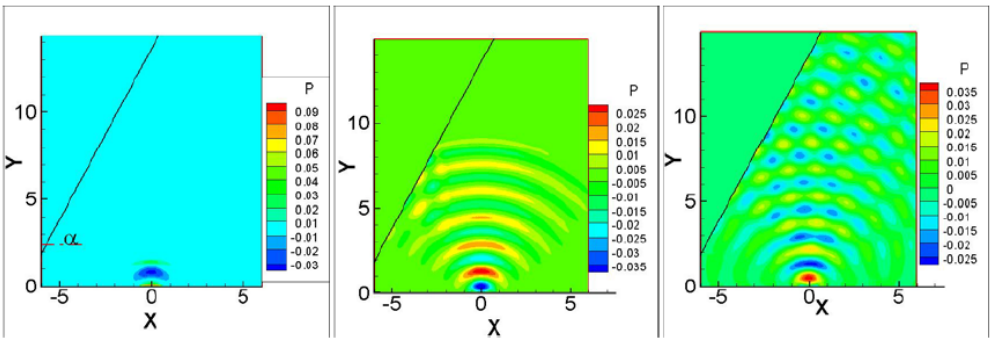

Figure 14: a) $t = 1.5$, b) $t = 9.4$, c) $t = 25.0$. Wave generated by a baffled piston and reflected by a solid wall.

Popescu, Shyy and Tai [11] conclude that, based on the test cases, the presented approach can be effective for acoustic problems with complex geometry. Also they conclude that the computational overhead of the cut-cell method is modest, because much computations in the vicinity of the boundary have to be done once (because the geometry is fixed).

3.3 Future work

In this report several numerical methods has been presented in order to tackle computational acoustic problems. Also a testcase has been presented to test these methods. The results of this testcase are satisfactory and the conclusion is that finite volume 6/4 OPC spatial discretization and 4-6-LDDRK time integration in combination with the cut-cell method can be an effective approach for acoustic problems. Further investigation is needed to confirm this.

3.3.1 Proposals

It has been derived that the 6/4 OPC and 4-6-LDDRK schemes have both fourth order accuracy. Also the cut-cell method uses fourth order interpolation methods to handle the complex geometry. Because there is no analytical solution of this testcase the order of accuracy cannot be determined explicitly. However, it is important to know what the order of accuracy is in practice. Another important issue is the impact of interpolation in the cut-cell procedure on the order of accuracy of the complete method. Two proposals are presented in order to investigate the order of accuracy and improve the numerical solution.

1. In order to determine the order of accuracy Richardson extrapolation can be used. Richardson extrapolation is based on numerical experiments. Also the impact of interpolation in the cut-cell procedure can be investigated by these numerical experiments.

2. Richardson extrapolation can also be used to improve the accuracy of the solution. Shyy and Garbey [13] describe Richardson extrapolation and also present a least square extrapolation method, which is more robust and numerically efficient.

3.3.2 Richardson Extrapolation

Let $N(h)$ be an approximation of M. Then the error of this approximation can be written as follows:

$$M - N(h) = C_1 h^{p_1} + C_2 h^{p_2} + ... \tag{103}$$

where $C_i \in \mathbb{R}$ and $p_i \in \mathbb{N}$ with $0 \leq p_1 < p_2 < ...$
When h is small, (103) can be approximated by:

$$M - N(h) = Ch^p. \tag{104}$$

Now, this equation can be written down for h, $\frac{h}{2}$ and $\frac{h}{4}$, which gives the following system:

$$\begin{array}{l} M - N(h) = Ch^p, \\ M - N(\frac{h}{2}) = C\left(\frac{h}{2}\right)^p, \\ M - N(\frac{h}{4}) = C\left(\frac{h}{4}\right)^p. \end{array} \tag{105}$$

After subtracting the second equation from the first, the third from the second and dividing these expressions the following is obtained:

$$\frac{N(\frac{h}{2}) - N(h)}{N(\frac{h}{4}) - N(\frac{h}{2})} = 2^p. \tag{106}$$

From this equation the order of accuracy p can be determined.
By subtracting the second and third equation of (105), C can be determined:

$$C = \frac{N(\frac{h}{4}) - N(\frac{h}{2})}{(\frac{h}{2})^p(1 - (\frac{1}{2})^p)}. \tag{107}$$

From the third equation of (105) an improvement of the solution accuracy can be derived:

$$N_{impr} = N(\frac{h}{4}) + C\left(\frac{h}{4}\right)^p. \tag{108}$$

This can be written as follows:

$$N_{impr} = \frac{2^p N(\frac{h}{4}) - N(\frac{h}{2})}{(2^p - 1)}. \tag{109}$$

This procedure can easily be extended to higher dimensions.
Shyy and Garbey [13] developed a least square extrapolation, which has the same goal as Richardson extrapolation, but which is more robust and efficient.

4 References

[1] C.K.W. Tam and J.C. Webb, "Dispersion-Relation-Preserving Finite Difference Schemes for Computational Acoustics", Journal of Computational Acoustics, Vol. 107, p. 262-281, 1993

[2] M. Popescu, "A Finite Volume, Cartesian Grid Method for Acoustic Problems with Complex Geometry, A Research Proposal", 2004

[3] W. Shyy and M. Popescu, "Assessment of Dispersion-Relation-Preserving and Space-Time Schemes for Wave Equations", American Institute of Aeronautics and Astronautics, 2002

[4] G. Ashcroft and X. Zhang, "Optimized Prefactored Compact Schemes", Journal of Computational Physics, Vol. 190, p. 459-477, 2003

[5] R. Hixon and E. Turkel, "High-Accuracy Compact MacCormack-Type Schemes for Computational Aeroacoustics", NASA CR 1998-208672, 1998

[6] J.W. Kim and D.J. Lee, "Optimized Compact Finite Difference Schemes with Maximum Resolution", AIAA Journal, Vol. 34, p. 887, 1996

[7] F.Q. Hu, M.Y. Hussaini and J.L. Manthey, "Low Dissipation and Dispersion Runge-Kutta for Computational Acoustics", Journal of Computational Physics, Vol. 124, p. 177-191, 1996

[8] G.B. Whitham, "Linear and nonlinear waves", Wiley, New York, 1974

[9] D.T. Blackstock, "Fundamentals of Physical Acoustics", Wiley, New York, 2000

[10] M.E. Goldstein, "Aeroacoustics", McGraw-Hill, New York, 1976

[11] M. Popescu, C. Tai and W. Shyy, "A Finite Volume-Based High Order Cartesian Cut-Cell Method for Computational Aeroacoustics", 11^{th} AIAA/CEAS Aeroacoustics Conference, Monterey, California, 2005

[12] M. Popescu, W. Shyy and M. Garbey, "A Study of Dispersion-Relation-Preserving and Optimized Prefactored Compact Schemes for Wave Equations", AIAA paper 2004-0519, 2004

[13] W. Shyy and M. Garbey, "A least square extrapolation method for improving solution accuracy of PDE computations", Journal of Computational Physics, Vol. 186, p. 1-23, 2003

5 Appendix

The equivalence is shown for the fourth order Runge-Kutta scheme and the following ordinary differential equation:

$\frac{du}{dt} = F(u)$,

where $F(u)$ is a linear operator.

1. Standard notation:

$k_1 = \Delta t F(u^n)$,
$k_2 = \Delta t F(u^n + \frac{1}{2}k_1)$,
$k_3 = \Delta t F(u^n + \frac{1}{2}k_2)$,
$k_4 = \Delta t F(u^n + k_3)$,
$u^{n+1} = u^n + \frac{1}{6}(k_1 + 2k_2 + 2k_3 + k_4)$.

2. Notation used in this work:

$K_1 = \Delta t F(u^n)$,
$\vdots$
$K_i = \Delta t F(u^{(i-1)})$,
$u^{(i)} = u^n + b_i K_i, \qquad i = 1...p,$
$\vdots$
$u^{n+1} = u^{(p)}$,
where $b_p = 1$ and $p = 4$ for fourth order.

Writing out both:

1. $u^{n+1} = u^n + \frac{1}{6}(k_1 + 2k_2 + 2k_3 + k_4) =$
$u^n + \frac{1}{6}(\Delta t F(u^n) + 2\Delta t F(u^n + \frac{1}{2}k_1) + 2\Delta t F(u^n + \frac{1}{2}k_2) + \Delta t F(u^n + k_3)) =$
$u^n + \frac{1}{6}(6\Delta t F(u^n) + \Delta t F(k_1) + \Delta t F(k_2) + \Delta t F(k_3)) =$
$u^n + \frac{1}{6}(6\Delta t F(u^n) + \Delta t^2 F(F(u^n)) + \Delta t^2 F(F(u^n + \frac{1}{2}k_1)) +$
$\Delta t^2 F(F(u^n + \frac{1}{2}k_2))) =$
$u^n + \frac{1}{6}(6\Delta t F(u^n) + \Delta t^2 FF(u^n) + \Delta t^2 FF(u^n) + \Delta t^2 FF(\frac{1}{2}k_1) +$
$\Delta t^2 FF(u^n) + \Delta t^2 FF(\frac{1}{2}k_2)) =$
$u^n + \frac{1}{6}(6\Delta t F(u^n) + 3\Delta t^2 FF(u^n) + \frac{1}{2}\Delta t^3 FFF(u^n) +$
$\frac{1}{2}\Delta t^3 FFF(u^n + \frac{1}{2}k_1)) =$
$u^n + \frac{1}{6}(6\Delta t F(u^n) + 3\Delta t^2 FF(u^n) + \Delta t^3 FFF(u^n) + \frac{1}{4}\Delta t^4 FFFF(u^n)) =$
$u^n + \Delta t F(u^n) + \frac{1}{2}\Delta t^2 FF(u^n) + \frac{1}{6}\Delta t^3 FFF(u^n) + \frac{1}{24}\Delta t^4 FFFF(u^n)$.

2. $u^{n+1} = u^{(p)} = u^n + b_4 K_4 = u^n + b_4 \Delta t F(u^{(3)}) = u^n + b_4 \Delta t F(u^n + b_3 K_3) =$
$u^n + b_4 \Delta t F(u^n) + b_4 b_3 \Delta t F(\Delta t F(u^{(2)})) = u^n + b_4 \Delta t F(u^n) +$
$b_4 b_3 \Delta t^2 FF(u^n + b_2 K_2) =$
$u^n + b_4 \Delta t F(u^n) + b_4 b_3 \Delta t^2 FF(u^n) + b_4 b_3 b_2 \Delta t^2 FF(\Delta t F(u^{(1)})) =$
$u^n + b_4 \Delta t F(u^n) + b_4 b_3 \Delta t^2 FF(u^n) + b_4 b_3 b_2 \Delta t^3 FFF(u^n + b_1 K_1) =$
$u^n + b_4 \Delta t F(u^n) + b_4 b_3 \Delta t^2 FF(u^n) + b_4 b_3 b_2 \Delta t^3 FFF(u^n) + b_4 b_3 b_2 b_1 \Delta t^4 FFFF(u^n)$.

With:

$b_4 = 1$, $b_3 = \frac{1}{2}$, $b_2 = \frac{1}{3}$, $b_1 = \frac{1}{4}$,

this notation is equivalent with the standard Runge-Kutta fourth order notation. The implementation of this notation is easier and needs less storage than the standard Runge-Kutta.